THE RADON TRANSFORM FOR TERAHERTZ COMPUTED TOMOGRAPHY INCORPORATING THE BEAM SHAPE

Lars-Paul Lumbeeck, Pavel Paramonov, Jan Sijbers, Jan De Beenhouwer

imec-VisionLab, Department of Physics, University of Antwerp, Belgium

ABSTRACT

In this paper, we study the influence of the beam shape of Terahertz (THz) radiation on the image formation in THz computed tomography and how to account for it in the reconstruction process. This is accomplished by first considering the beam shape in the forward projection using a modified Radon transform and then inverting this transform to construct new inversion techniques. Simulation experiments show that, compared to conventional back projection, directly incorporating the beam shape in the Radon transform can significantly improve image quality in terms of the mean squared error and the Structural Similarity Index.

***Index Terms*—** Computed tomography, Terahertz imaging, Radon transform, Beam shape

1. INTRODUCTION

THz tomography has a wide range of application domains, including the study of biological materials (e.g., human breast tumors [1], human bones [2]), artwork and ancient artefacts examination [3–5], as well as security and surveillance [6–8]. It is a non-invasive and non-destructive imaging method and is, unlike X-ray radiation, non-ionizing.

A common projection model in X-ray CT is the Radon transform [9], and most CT reconstruction methods are based on the mathematics of this transform. When this model is applied for THz radiation, the wave-like nature of the radiation needs to be considered due to the larger wavelength compared to X-ray. Effects such as refraction, reflection, diffraction and the THz beam shape need to be taken into account when dealing with THz radiation.

This paper studies specifically the effects of the THz beam profile on simulated sinogram data. To compensate for the effects caused by the shape of the THz beam, we incorporate the beam shape into a modified Radon Transform. The inverse of this modified transform is then used to define a reconstruction method that accounts for the THz beam shape.

2. THZ RADON TRANSFORM

In X-ray CT, the 2D Radon transform is defined as follows [9]:

$$R_\theta(\rho) = \iint_{-\infty}^{+\infty} f(x,y)\delta(\rho - x\cos\theta - y\sin\theta)dxdy \qquad (1)$$

with θ the projection angle and ρ the offset of the shift along the projection line. In this model, the beam is approximated by a line with zero width, which is a good approximation if the wavelength of the radiation is small compared to the size of the object. In THz tomography, this assumption no longer holds, and the beam shape must be considered [10]. The intensity profile of the beam in THz imaging typically resembles a Gaussian distribution [11], which can be described as follows:

$$I(r,z) = I_0 \left(\frac{w_0}{w(z)}\right)^2 e^{-\frac{2r^2}{w^2(z)}} \qquad (2)$$

with r the radial distance from the center axis of the beam, z the axial distance from the beam's focus, and I_0 the intensity at the center of the beam. The function $w(z)$ represents the beam's width and is given by:

$$w(z) = w_0\sqrt{1 + \left(\frac{z}{z_R}\right)^2} \qquad (3)$$

with $w_0 = w(0)$ the beam's waist radius, λ the wavelength and z_R the Rayleigh range ($z_R = \frac{\pi w_0^2}{\lambda}$). For simplicity, we proceed in 2D, thereby assuming that the object $f(x,y,z)$ is constant in the z-direction, which is equivalent to using the new 2D beam profile (Fig. 1):

$$I^{2D}(x,y) = I_0\sqrt{\frac{\pi}{2}}\frac{w_0^2}{w(y)}e^{-\frac{2x^2}{w^2(y)}} \qquad (4)$$

To account for the beam shape, we alter the Radon transform by convolving the image $f(x,y,z)$ with the Gaussian beam intensity, giving us the THz Radon transform [11]:

$$p_\theta(\rho) = \iint f * I_\theta^{2D}(x,y)\delta(\rho - x\cos\theta - y\sin\theta)dxdy \qquad (5)$$

with $*$ a 1D convolution perpendicular to the projection direction and I_θ^{2D} the intensity profile rotated over an angle of θ which defines the projection direction (Fig. 2).

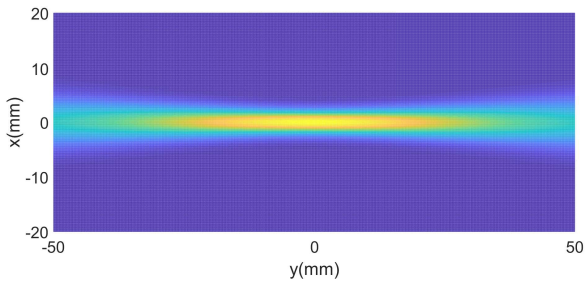

Fig. 1: Intensity profile (in mm) for a beam with wavelength λ = 1 mm and beam width w_0 = 3 mm.

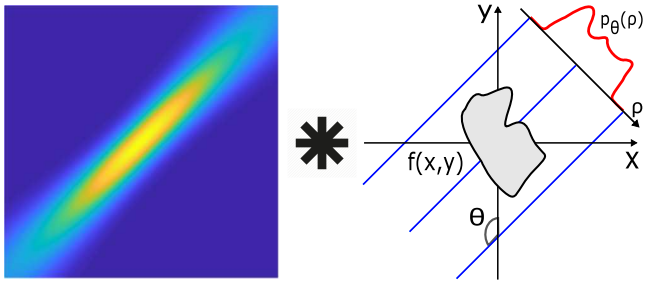

Fig. 2: Visualisation of the THz Radon transform.

As an example, we apply this transform to a (250×250 pixels) phantom consisting of 4 circles over 250 different angles (over 180 degrees) to generate the sinogram $p_\theta(\rho)$. The goal now is to find an inversion method that reconstructs the original image $f(x, y)$ from $p_\theta(\rho)$ (Fig. 3).

3. RECONSTRUCTION

3.1. Constant beam

In the limit where the Rayleigh length goes to infinite, finding the inverse of the THz Radon transform is fairly simple, because then the width of the intensity becomes constant:

$$\lim_{z_R \to \infty} I^{2D}(x, y) = I_0 \sqrt{\frac{\pi}{2}} w_0 e^{-\frac{2x^2}{w_0^2}} = I^{2D}(x, 0) \quad (6)$$

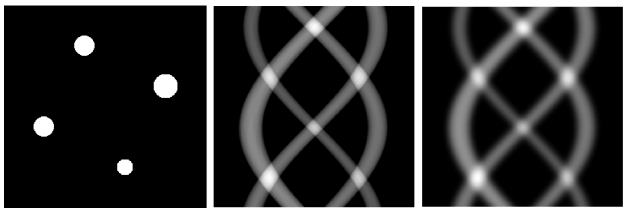

(a) (b) (c)

Fig. 3: (a) Example image consisting of 4 circles with diameters ranging from 8 mm to 12 mm, (b) Sinogram calculated with the Radon transform, (c) Sinogram calculated with the THz radon transform (for a beam with wavelength λ = 1 mm and w_0 = 3 mm).

Now $I^{2D}(x, y)$ is independent of y and it is possible to invert Eq. (5):

$$f(x,y) = \frac{1}{4\pi^2} \int_0^\pi \int_{-\infty}^{+\infty} |\omega| \exp\left(i\omega \cos\theta x + i\omega \sin\theta y\right) \cdot \frac{\int p_\theta(\rho) e^{-i\omega\rho} d\rho}{\int I^{2D}(\tau, 0) e^{-i\omega\tau} d\tau} d\omega d\theta \quad (7)$$

Note that Eq. (7) is a combination of a deconvolution with $I^{2D}(\tau, 0)$ and the inverse Radon transform (also known as the filtered back projection (FBP) [12]). So if we define $p'_\theta(\rho')$ as the sinogram deconvolved with $I^{2D}(\tau, 0)$ we can write Eq. (7) in the two steps:

$$f(x,y) = \frac{1}{4\pi^2} \int_0^\pi \int_{-\infty}^{+\infty} |\omega| \exp\left(i\omega \cos\theta x + i\omega \sin\theta y\right) \left(\int e^{-i\rho'\omega} p'_\theta(\rho') d\rho' \right) d\omega d\theta \quad (8)$$

With:

$$p'_\theta(\rho') = \frac{1}{2\pi} \int e^{i\rho'\nu} \frac{\int p_\theta(\rho) e^{-i\nu\rho} d\rho}{\int I^{2D}(\tau, 0) e^{-i\nu\tau} d\tau} d\nu \quad (9)$$

3.2. General case

When the Rayleigh length is comparable to w_0 or smaller, finding the inverse transformation is more challenging, because of the beam shape's (I^{2D}) dependence on y. We simplify this problem, by first defining $p'_\theta(\rho')$ again as our sinogram deconvolved with $I^{2D}(\tau, 0)$ (see Eq. (9)) and then applying the inverse Radon transform, resulting in $h(x, y)$, the solution in the constant beam limit ($z_R \to \infty$):

$$h(x,y) = \frac{1}{4\pi^2} \int_0^\pi \int_{-\infty}^{+\infty} |\omega| \exp\left(i\omega \cos\theta x + i\omega \sin\theta y\right) \cdot \left(\int e^{-i\omega\rho'} p'_\theta(\rho') d\rho' \right) d\omega d\theta \quad (10)$$

The relation between $h(x, y)$ and $f(x, y)$ can then be expressed as:

$$h(x,y) = \sqrt{\frac{2}{\pi}} \frac{z_R}{w_0} \iint_{-\infty}^{+\infty} \delta(y'(y' - y) + x'(x' - x)) \cdot \exp\left(-\frac{2z_R^2 (x - x')^2}{w_0^2 y'^2} \right) f(x', y') dx' dy' \quad (11)$$

The variable $h(x, y)$ can already be calculated from the sinogram $p_\theta(\rho)$, so to find $f(x, y)$ we only need to inverse the transform described by Eq. (11). The inverse of this transformation (let us call it H) is not obvious, but for now we can at least find the adjoint transformation applied to an arbitrary function $g(x, y)$:

$$H^T g\ (x,y) = \sqrt{\frac{2}{\pi}}\frac{z_R}{w_0}\iint_{-\infty}^{+\infty} \delta(y(y-y') + x(x-x')) \cdot \exp\left(-\frac{2z_R^2(x'-x)^2}{w_0^2 y^2}\right) g(x',y')dx'dy' \tag{12}$$

which will be used in the next subsection.

3.3. Correction matrix H

The structure of Eq. (11) is similar to that of the Radon transform, so the same iterative methods will be employed to calculate $f(x,y)$ from $h(x,y)$. For this, a matrix $\boldsymbol{H}$ representing the transform H is needed, but first we take a closer look at the delta function in the transform. The delta function describes a circle going through the coordinates $(0,0)$ and (x,y) and is quite difficult to construct a matrix with, as the arc lengths of circles need to be calculated.

The easier option is to use Eq. (12) to create $\boldsymbol{H^T}$ instead [13]. Here, the delta function describes straight lines passing through (x,y) , perpendicular to the radial direction in (x,y) (Fig. 4).

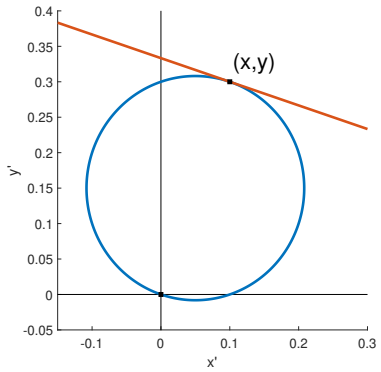

Fig. 4: Path of the line integration of H (blue) and H^T (red) for (x,y) = (0.1,0.3).

3.4. Reconstruction methods

When the matrix $\boldsymbol{H}$ is constructed, there are 3 different methods for reconstruction possible. The first one (method 1) is by applying Eq. (10) to $\boldsymbol{p}$ ($p_\theta(\rho)$ discretized) to find $\boldsymbol{h}$ ($h(x,y)$ discretized) and then using $\boldsymbol{H}$ to iteratively approximate $\boldsymbol{x}$ ($f(x,y)$ discretized). However, keep in mind that Eq. (10) is a combination of a deconvolution with $I^{2D}(\tau,0)$ and the inverse Radon transform. Therefore, a second method (method 2) consists of rewriting $\boldsymbol{W}$, the matrix describing the THz forward projection, as a combination of the matrix $\boldsymbol{C}$ (representing the convolution with $I^{2D}(x,0)$), an X-ray forward projection $\boldsymbol{W}_{\text{X-ray}}$ and a correction matrix $\boldsymbol{H}$, all of which can be written as sparse matrices:

$$\boldsymbol{Wx} = \boldsymbol{CW}_{\text{X-ray}}\boldsymbol{Hx} = \boldsymbol{p} \tag{13}$$

Solving this linear system will result in the desired reconstruction, for method 1 that system is:

$$\boldsymbol{Hx} = \boldsymbol{W}_{\text{X-ray}}^{-1}\boldsymbol{C}^{-1}\boldsymbol{p} \tag{14}$$

The problem with the second approach is that the matrix $\boldsymbol{C}$ causes this system to converge very slowly. The best method seems to be the middle ground between method 1 and 2, which is deconvolving $\boldsymbol{p}$ with $I^{2D}(\tau,0)$ and then using $\boldsymbol{W}_{\text{X-ray}}$ and $\boldsymbol{H}$ to iteratively solve the linear equation:

$$\boldsymbol{W}_{\text{X-ray}}\boldsymbol{Hx} = \boldsymbol{C}^{-1}\boldsymbol{p} \tag{15}$$

to find $\boldsymbol{x}$. Which is equivalent to stating that $\boldsymbol{C^{-1}}$ is a preconditioner for our problem.

4. RESULTS

Our reconstruction methods are compared in Fig. 5. First a blurred sinogram is generated with the THz Radon transform and then the original example image is reconstructed with X-ray FBP and the 3 proposed methods.

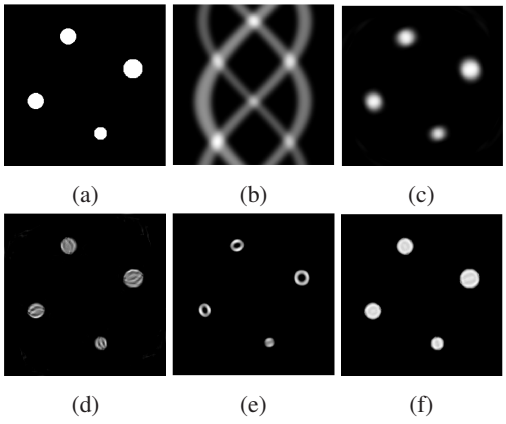

Fig. 5: (a) Example image from Fig. 3, (b) Sinogram calculated with the THz radon transform (for a beam with wavelength λ = 1 mm and w_0 = 3 mm), (c) blurred sinogram backprojected using X-ray FBP, (d) using method 1, (e) 2 and (f) 3.

To evaluate our reconstruction methods the mean squared error (MSE) and the Structural Similarity Index (SSIM) [14] of each image are compared to the ground truth (Fig. 5(a)).

Image	MSE	SSIM
FBP	0.0057	0.88
Method 1	0.0034	0.93
Method 2	0.0280	0.94
Method 3	0.0013	0.98

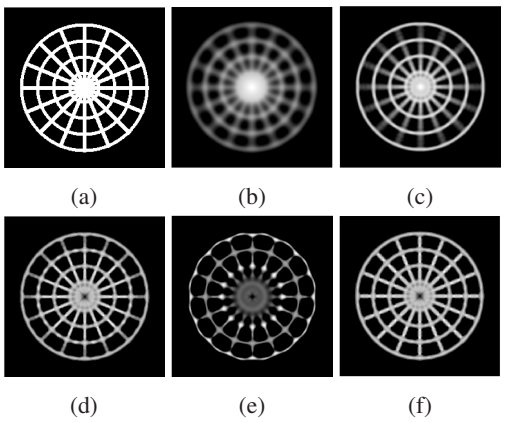

Fig. 6: (a) Example image consisting of 4 concentric circles and 8 radial lines creating a spider web , (b) Blurred sinogram backprojected using X-ray FBP, (c) using the constant beam reconstruction method, (d) using method 1, (e) 2 and (f) 3 (using a beam with wavelength λ = 1 mm and w_0 = 3 mm).

From the MSE, SSIM and visual comparison, it is clear that all 3 methods reduce the blurring caused by the beam shape. However, in the process, method 1 and 2 have created extra artefacts, especially method 2, which has a higher MSE than even FBP. Method 3 seems to perform best. Next, the radial and angular component of the reconstruction methods on a spider web-like phantom are tested (Fig. 6).

The result from the constant beam method (which is the same as method 1 without compensating for H) indicates that H does not have a large influence on the radial component of the forward projection. This can be explained by looking at the path of the delta function (Fig. 4). Consequently, a large difference between the concentric circles of method 1 and 3 is not expected. Due to its slow convergence, method 2 performed worst. To quantify the convergence rates, the condition number κ was calculated for each method for a forward projection with a resolution of 50×50 and 50 angles. κ_1 = $3.9{\cdot}10^4$, κ_2 = $4.4{\cdot}10^{17}$ and κ_3 = $2.0{\cdot}10^{10}$, clearly demonstrating the slowness of method 2.

Image	MSE	SSIM
FBP	0.071	0.57
Constant beam	0.035	0.78
Method 1	0.025	0.86
Method 2	0.119	0.69
Method 3	0.020	0.85

Another noticeable aspect of the methods is the appearance of a black spot in the center of the image. This is likely caused by the approximations made by discretizing H^T and may therefore be solved by constructing the matrix $\boldsymbol{H}$ instead.

5. DISCUSSION

In the limit where the Rayleigh range (z_R) approaches infinity (resulting in a constant beam width) we succeeded at finding the inverse of the THz Radon transform, which turned out to be an adjusted form of FBP (constant beam approximation). In the case of a non-constant beam, we were able to split the forward projection into three parts: a convolution $\boldsymbol{C}$, an ordinary forward projection $\boldsymbol{W}_{\text{X-ray}}$ and a correction matrix $\boldsymbol{H}$. The inverse of $\boldsymbol{C}$ and $\boldsymbol{W}_{\text{X-ray}}$ are calculable, but the inverse of $\boldsymbol{H}$ is not, resulting in three methods to approximate the original image. Method 1: apply the constant beam method first and then use $\boldsymbol{H}$ and $\boldsymbol{H}^{\boldsymbol{T}}$ to improve the approximation iteratively; method 2: write all 3 components as sparse matrices to iteratively approximate the image; method 3: use $\boldsymbol{C}^{-1}$ as a preconditioner and then reconstruct the image with the matrices $\boldsymbol{W}_{\text{X-ray}}$ and $\boldsymbol{H}$.

The constant beam approximation is fast, but only works well for beams of which the Rayleigh length is large compared to the beam's waist radius or when the image is close to constant in the angular direction. With method 1, this approximation can be quickly improved, but this method does not converge well to the ground truth, which is more noticeable the more iterations are used. Method 2 should theoretically give the best results but is not viable because of its extremely slow convergence. Method 3 also has a high condition number compared to method 1, but not nearly as big as for method 2 and seems to be the most reliable of the methods consistently resulting in good reconstructions.

6. CONCLUSION

In this paper, a modified version of the Radon transform is proposed that incorporates the (Gaussian) beam shape in THz CT. Additionally, this beam shape is accounted for in the reconstruction, by using the inverse of this THz Radon transform. If the beam width is constant, the inverse transform exists, but if the beam width changes, iterative methods are needed. This is done by splitting the projection into three parts, a convolution, an ordinary forward projection and a correction. The inverse of the convolution and the projection transformations are known, but the inverse of the correction is not. This results in three different methods for reconstruction depending on which part is done iteratively. The performance of these methods were then quantified in terms of accuracy and speed of convergence. The overall best method seems to be using the convolution as a preconditioner and using iterative methods to approximate the reconstruction.

7. REFERENCES

[1] Anthony J. Fitzgerald, Vincent P. Wallace, Mercedes Jimenez-Linan, Lynda Bobrow, Richard J. Pye,

Anand D. Purushotham, and Donald D. Arnone, "Terahertz pulsed imaging of human breast tumors," *Radiology*, vol. 239, no. 2, pp. 533–540, 2006.

[2] Maryelle Bessou, Bruno Chassagne, Jean-Pascal Caumes, Christophe Pradère, Philippe Maire, Marc Tondusson, and Emmanuel Abraham, "Three-dimensional terahertz computed tomography of human bones," *Applied optics*, vol. 51, no. 28, pp. 6738–6744, 2012.

[3] J. Labaune, J.B. Jackson, S. Pages-Camagna, M. Menu, and G.A. Mourou, "Terahertz investigation of Egyptian artifacts," in *35th International Conference on Infrared, Millimeter, and Terahertz Waves*. IEEE, 2010, pp. 1–3.

[4] Jean-Pascal Caumes, Ayesha Younus, Simon Salort, Bruno Chassagne, Benoît Recur, Anne Ziéglé, Alain Dautant, and Emmanuel Abraham, "Terahertz tomographic imaging of XVIIIth Dynasty Egyptian sealed pottery," *Applied optics*, vol. 50, no. 20, pp. 3604–3608, 2011.

[5] J. Bianca Jackson, John Bowen, Gillian Walker, Julien Labaune, Gerard Mourou, Michel Menu, and Kaori Fukunaga, "A survey of terahertz applications in cultural heritage conservation science," *IEEE Transactions on Terahertz Science and Technology*, vol. 1, no. 1, pp. 220–231, 2011.

[6] Holger Quast and Torsten Loffler, "3D-terahertz-tomography for material inspection and security," in *2009 34th International Conference on Infrared, Millimeter, and Terahertz Waves*. IEEE, 2009, pp. 1–2.

[7] Panagiotis C. Theofanopoulos and Georgios C. Trichopoulos, "A novel THz radar imaging system using the radon transform," in *2017 IEEE International Symposium on Antennas and Propagation & USNC/URSI National Radio Science Meeting*. IEEE, 2017, pp. 1513–1514.

[8] Panagiotis C. Theofanopoulos, Mahmoud Sakr, and Georgios C. Trichopoulos, "Multistatic terahertz imaging using the radon transform," *IEEE Transactions on Antennas and Propagation*, vol. 67, no. 4, pp. 2700–2709, 2019.

[9] J. Radon, "Uber die bestimmung von funktionen durch ihre integralwerte längs gewisser mannigfaltigkeiten," *Ber. Verh. Saechs. Akad. Wiss. Leipzig Math. Phys. Kl.*, vol. 69, pp. 262, 1917.

[10] J.P. Guillet, B. Recur, I. Manek-Hönninger, J.C. Delagnes, W Benharbone, P Desbarats, J.P. Domenger, L. Canioni, and P. Mounaix, "3D-Terahertz Tomography using a more realistic beam propagation model applied to different image reconstruction methods," pp. 1–2, 2012.

[11] Benoît Recur, Jean-Paul Guillet, Inka Manek-Hönninger, Jean-Christophe Delagnes, William Benharbone, Pascal Desbarats, Jean-Philippe Domenger, Lionel Canioni, and Patrick Mounaix, "Propagation beam consideration for 3D THz computed tomography," *Optics express*, vol. 20, no. 6, pp. 5817–5829, 2012.

[12] Gabor T. Herman, "Image reconstruction from projections," *The fundamental of computerized tomography*, pp. 260–276, 1980.

[13] Wim Van Aarle, Willem Jan Palenstijn, Jan De Beenhouwer, Thomas Altantzis, Sara Bals, K. Joost Batenburg, and Jan Sijbers, "The ASTRA Toolbox: A platform for advanced algorithm development in electron tomography," *Ultramicroscopy*, vol. 157, pp. 35–47, 2015.

[14] Zhou Wang, Alan C. Bovik, Hamid R. Sheikh, and Eero P. Simoncelli, "Image quality assessment: from error visibility to structural similarity," *IEEE transactions on image processing*, vol. 13, no. 4, pp. 600–612, 2004.